Brain, Behavior, & Immunity - Health 32 (2023) 100662

Contents lists available at ScienceDirect

Brain, Behavior, & Immunity - Health

journal homepage: www.editorialmanager.com/bbih/default.aspx

Cytoarchitectureal changes in hippocampal subregions of the NZB/W F1 mouse model of lupus

J.-M. Graïc [a], L. Finos [b], V. Vadori [e], B. Cozzi [a], R. Luisetto [c], T. Gerussi [a], Gatto M [d], A. Doria [d], E. Grisan [e], L. Corain [f], A. Peruffo [a,*]

[a] Department of Comparative Biomedicine and Food Science, University of Padova, 35020, Italy
[b] Department of Statistical Sciences, University of Padova, Padova, 35100, Italy
[c] Department of Surgery, Oncology and Gastroenterology, University of Padova, Padova, 35100, Italy
[d] Rheumatology Unit, Department of Medicine (DIMED), University of Padova, Padova, 35100, Italy
[e] School of Engineering, London South Bank University, London, SE1 0AA, UK
[f] Department of Management and Engineering, University of Padova, Vicenza, 36100, Italy

ARTICLE INFO

Keywords:
Neurolupus
NZB/NZW F1
Lupus model
Hippocampus
Cytoarchitecture
Multivariate analysis

ABSTRACT

Over 50% of clinical patients affected by the systemic lupus erythematosus disease display impaired neurological cognitive functions and psychiatric disorders, a form called neuropsychiatric systemic lupus erythematosus. Hippocampus is one of the brain structures most sensitive to the cognitive deficits and psychiatric disorders related to neuropsychiatric lupus. The purpose of this study was to compare, layer by layer, neuron morphology in lupus mice model NZB/W F1 *versus* Wild Type mice.

By a morphometric of cells identified on Nissl-stained sections, we evaluated structural alterations between NZB/W F1 and Wild Type mice in seven hippocampal subregions: Molecular dentate gyrus, Granular dentate gyrus, Polymorph dentate gyrus, Oriens layer, Pyramidal layer, Radiatum layer and Lacunosum molecular layer. By principal component analysis we distinguished healthy Wild Type from NZB/W F1 mice. In NZB/W F1 mice hippocampal cytoarchitecture, the neuronal cells resulted larger in size and more regular than those of Wild Type. In NZB/W F1, neurons were usually denser than in WT. The Pyramidal layer neurons were much denser in Wild Type than in NZB/W F1. Application of principal component analysis, allowed to distinguish NZB/W F1 lupus mice from healthy, showing as NZBW subjects presented a scattered distribution and intrasubject variability.

Our results show a hypertrophy of the NZB/W F1 hippocampal neurons associated with an increase in perikaryal size within the CA1, CA2, CA3 region and the DG. These results help advance our understanding on hippocampal organization and structure in the NZB/W F1 lupus model, suggesting the hypothesis that the different subregions could be differentially affected in neuropsychiatric systemic lupus erythematosus disease. Leveraging an in-depth analysis of the morphology of neural cells in the hippocampal subregions and applying dimensionality reduction using PCA, we propose an efficient methodology to distinguish pathological NZBW mice from WT mice."

1. Introduction

Systemic Lupus Erythematosus (SLE) is an auto-immune disease that affects a variety of organ systems by altering the regulatory pathways of inflammation (Ghirardello et al., 2004), including the central nervous system (CNS) (Leung et al., 2016). Up to 75% of SLE patients show neurological symptoms involving a range of cognitive deficits, psychiatric disorders (Briani et al., 2009) and memory loss. This form is termed neuropsychiatric SLE (NPSLE). Beyond the existence of these symptoms, the full spectrum of NPSLE manifestation remains poorly understood (Schwartz et al., 2019). One of the brain regions most suspected to have marked NPSLE-related changes is the hippocampus. Critically involved in fundamental processes such as learning, emotions, spatial navigation and memory, the hippocampus is among the most studied neural systems in mammals. The *hippocampus proper* comprises the dentate gyrus (DG), CA1, CA2 and CA3 regions, each with their own cellular structure

* Corresponding author. Department of Comparative Biomedicine and Food Science, University of Padova, viale dell'Università 16, 35020 Legnaro PD, Italy.
E-mail address: antonella.peruffo@unipd.it (A. Peruffo).

https://doi.org/10.1016/j.bbih.2023.100662
Received 13 February 2023; Received in revised form 20 June 2023; Accepted 23 June 2023
Available online 6 July 2023

and distinctive functions. The three layers of the DG are the molecular layer (MoDG), granule cell layer (GrDG) and polymorph dentate gyrus (PoDG). Within the CA1, CA2 and CA3 regions, a number of layers are defined. The pyramidal layer (Py), the subregion in which the main cell types are pyramidal neurons, differing in terms of genetics, morphology, and connectivity (Merino-Serra et al., 2020). Deep to the Py is the *stratum oriens* (Or), a relatively cell-free subregion containing mostly fibers and some interneurons. Superficial to the Py is the *stratum radiatum* (Rad) and *stratum lacunosum-moleculare* (LMol) containing GABAergic interneurons, which play a critical role in modulating the dynamic activity in hippocampus networks (Jarsky et al., 2005).

Anatomical observations and lesioning experiments support the idea that the hippocampus is crucial in memory formation, especially the dentate gyrus (DG) area, while the CA3 area covers the encoding, storage and retrieval of memory (Hainmueller and Bartos, 2020). The hippocampus also plays a major role in the formation of declarative, spatial, and contextual memory, as well as in the processing of emotional information and stress response (Zaletel et al., 2016).

The widely used NZB/W F1 (NZBW) murine model offers an opportunity to bridge the gap between neurological deficits and histological lesions underlying NPSLE (Pikman et al., 2017). NZBW mice spontaneously develop generalized auto-immune inflammation providing a powerful translational model to approach human autoimmune disease.

The neuronal loss and reduced neuronal density found in NZBW hippocampi were comparable to those described in human NPSLE patients (Ballok et al., 2004). The same year, Kowal and colleagues (Kowal et al., 2004) demonstrated that systemic immune responses could cause cognitive impairment even in the absence of an inflammatory cascade and suggested that the antibodies gained access to the brain to bind preferentially to hippocampal neurons, causing neuronal death with resulting cognitive dysfunction and altered hippocampal metabolism. More recent works focused on cellular and network basis of cognitive processes, allowing further understanding of the hippocampus role in complex memories processes (Lisman et al., 2017).

By advance quantitative imaging and statistical methods, over a large number of cells, we would like to contribute to the debate with hard evidence. In order to study quantitatively the fine changes in neuronal changes, and to quantify structural differences in the cytoarchitecture of NZBW and WT mice we set up an automatic pipeline combining image analysis together with a statistical data analysis based on a multivariate, multi-aspect testing approach.

2. Materials and methods

2.1. Mice

A series of 11 NZB/W F1 female mice (22-week-old), purchased from (Harlan Laboratories, Envigo RMS, UD, Italy) and 5 wild type (WT) female mice were housed in the animal facility of the Department of Surgery, Oncology and Gastroenterology of the University of Padova, Padova, Italy. The housing conditions were controlled, with the temperature at 21–23 °C and a 12:12 h light: dark cycle. All animal studies were approved by the Institutional Animal Care and Use Committee of the Albert Einstein College of Medicine. Mice used in this study were littermates. The NZB/W mice used are hybrid of two inbred strains (NZB females X NZW males) that are genetically uniform and heterozygous only for the genes for which the two parental strains differ. The genetic heterozygosity is related to some dominant alleles wherewith the two parental mice strains contribute in the development of the typical lupus-like auto anti-bodies production. Probably due to estrogen action and as its observed in human, lupus syndrome in the NZB/W F1 strain is strongly biased in favor of female.

2.2. Assessment of lupus

Mice were monitored twice a week for the development of proteinuria and autoantibody titers. Urinary protein excretion was measured by dipstick analysis (Uristix; Bayer), where +1 is 30 mg/dl, +2 is 100 mg/dl, +3 is 300 mg/dl, and +4 is $\geq$ 2000 mg/dl (Supplementary Material Table 1). Active generalized SLE was present in all mice of the NZBW group, as determined by elevated serum anti-DNA antibodies and by the presence of glomerulonephritis. Mouse IgG anti-double stranded (ds) DNA antibody titers were determined by ELISA, as previously described in detail (Gatto et al., 2016, 2020). Similar ELISA protocols were also used for anti-chromatin, anti-cardiolipin and anti-N-methyl-D-aspartate receptor antibody ELISAs (Gatto et al., 2016, 2020). For details of weight, age, values of proteinuria and autoantibody titers analyzed in NZBW mice before death see (Supplementary Material Table 1).

2.3. Brain tissue preparation and Nissl staining

The mouse brains were fixed in a 10% formaldehyde solution. After fixation, the brains were processed for paraffin embedding. The brains were cut into 8-μm-thick coronal sections. From each sample, continuous brain sections were stained following a routine Nissl protocol (Corain et al., 2020). The topography of the hippocampal region was assessed by comparison with detailed stereotaxic mouse brain atlases (Paxinos and Franklin, 2012). For cytoarchitectural analysis of the hippocampus we selected the range from Bregma was from −2.80 mm to −3.40 mm. In order to evaluate the hippocampal regions extension, we Nissl stained one section every ten per mouse brain in both NZB/WF1 and wild type populations.

2.4. Image acquisition and topographical mapping of the hippocampal subregions

Nissl-stained sections were digitalized with a semi-automated microscope (D-Sight v2, Menarini Diagnostics, Italy) with the 20× objecive at the best focal plane. The layers of interest were manually segmented on each acquired image using a general-purpose image-editing software (GNU Image Manipulation Program, The GIMP Development Team, 2019). For details see (supplementary material, Fig. 1).

2.5. Automatic cell identification

Each neuron was identified and segmented through an automatic image analysis method applied on the Nissl-stained section (Grisan et al., 2018). The process identified the position and outline of the visible cells within the manually outlined regions. Briefly, a local space-varying threshold applied to the image separated the stained objects (foreground) from the background. From the local surface density of the foreground objects (mainly cells), a separation of the densest (with clustered and cluttered cells) and sparsest regions is obtained (Poletti et al., 2012; Grisan et al., 2018), and the potential cell cluster were then identified. All identified clusters underwent secondary analyses to separate the cells composing them.

2.6. Cells classification by shape type and morphometric descriptors setting

For each cell in each subregion data characterizing its shape and local relationship with surrounding cells were collected (Corain et al., 2020). These data broadly belong to three domains: Size, Regularity and Density (supplementary material, Table 2). Size regarding cell morphology, are composed by shape measurements (area, perimeter, major and minor axis length). Regularity delineate the domain that consider the parameter Extent and the parameters Solidity. Extent is defined as: Area/(Area of the bounding box); Solidity is defined as the proportion of the pixels in the convex hull that are also in the object;

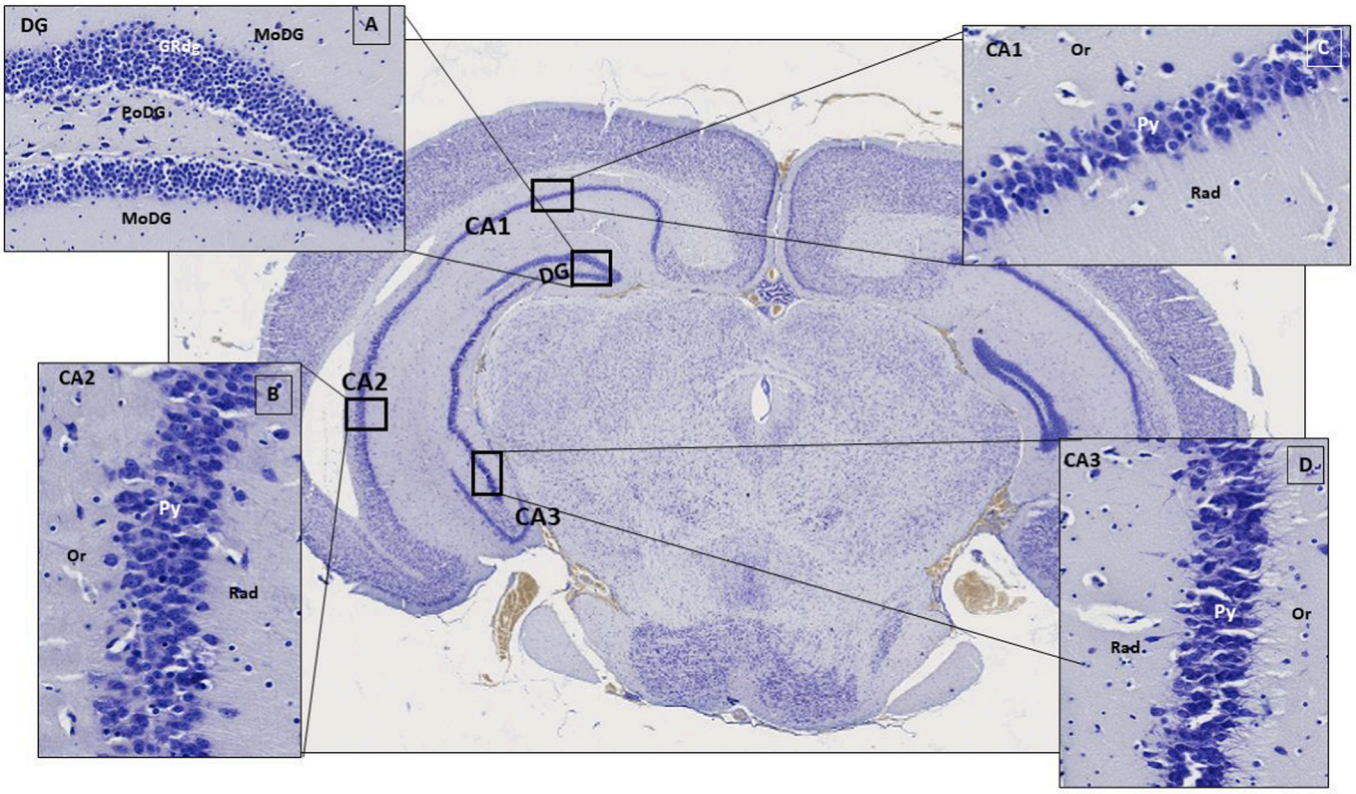

Fig. 1. A. Image of a Nissl stained coronal section of WT mouse brain showing the Dg, CA1, CA2 and CA3 hippocampal regions (×20). A. Enlargement of DG showing details of neuronal cells in the PoDG, GrDG and MoDG subregions. B. Enlargement of CA2 region showing details of neuronal cells in the Py, Or and Rad subregions. C. Enlargement of CA1 region showing details of neuronal cells in the Or, Py, Rad, subregions. D. Enlargement of CA3 region showing details of neuronal cells in the Py, Or and Rad subregion.

Table 1
Significant p-value combined by subregion and cells shape type for the domain Size with adjustment by multiplicity. The 1% statistically significant p-values are highlighted in bold.

Subregion	cell population Size difference p-value				
	Whole subregion	Round cells	Ellipsoid cells	Pyramidal cells	Complex cells
PoDG	0.0020	0.0030	0.0020	0.0010	0.0410
Or	0.0020	0.0020	0.0010	0.0030	0.0450
Py	0.0080	0.0040	0.0040	0.0020	0.1550
Rad	0.0050	0.0670	0.0020	0.0150	0.0090
LMol	0.0410	0.1530	0.0040	0.0290	0.9530
MoDG	0.0570	0.1530	0.0040	0.0290	0.9530
GrDG	0.0150	0.0010	0.0130	0.1120	0.0200

computed as Area/Convex Area. We defined "more regular" the neurons showing values closer to 1 of Extent and Solidity (cells show a rounded shape) in comparison to the lower values of these parameters (cells tend to be farther from the round shape). Density characterizes the context neighboring each cell by counting the number of cells within a radius of 50 μm or within 100 μm from the cell under analysis. Density descriptors are an absolute number of neighbor cells around a given cell. All neural cells were grouped in 4 categories defined by their shape: pyramidal, round, ellipsoid and complex. The total number of cells analyzed for the NZBW mice population and for the Wild Type mice population, in each subregions separately for cell shape is reported in the supplementary material. For details see (supplementary material, Table 2, Table 3 and Fig. 2).

Table 2
Statistically significant p-value combined by subregion and cells shape type for the Regularity domain with adjustment by multiplicity. The 1% statistically significant p-values are highlighted in bold.

Subregion	cell population Regularity difference p-value				
	Whole subregion	Round cells	Ellipsoid cells	Pyramidal cells	Complex cells
PoDG	0.0010	0.0010	0.0010	0.0040	0.3570
Or	0.0010	0.0010	0.0030	0.0010	0.5070
Py	0.0010	0.0140	0.0010	0.0010	0.0840
Rad	0.0010	0.0010	0.0040	0.0010	0.8310
LMol	0.0010	0.0010	0.0010	0.0010	0.2690
MoDG	0.0010	0.0030	0.0030	0.0010	0.0900
GrDG	0.0010	0.0250	0.0510	0.0510	0.2490

Table 3
Statistically significant p-value combined by subregion and cells shape type for the Density domain with adjustment by multiplicity. The 1% statistically significant p-values are highlighted in bold.

Subregion	cell population Density difference p-value				
	Whole subregion	Round cells	Ellipsoid cells	Pyramidal cells	Complex cells
PoDG	0.2330	0.5490	0.4430	0.0550	0.2350
Or	0.0240	0.0200	0.0110	0.0070	0.2210
Py	0.0090	0.0030	0.0040	0.0080	0.0190
Rad	0.0080	0.0030	0.0040	0.0080	0.0080
LMol	0.0090	0.0020	0.0020	0.0020	0.6990
MoDG	0.0090	0.0060	0.0020	0.0020	0.1410
GrDG	0.2330	0.1530	0.0960	0.4110	0.0960

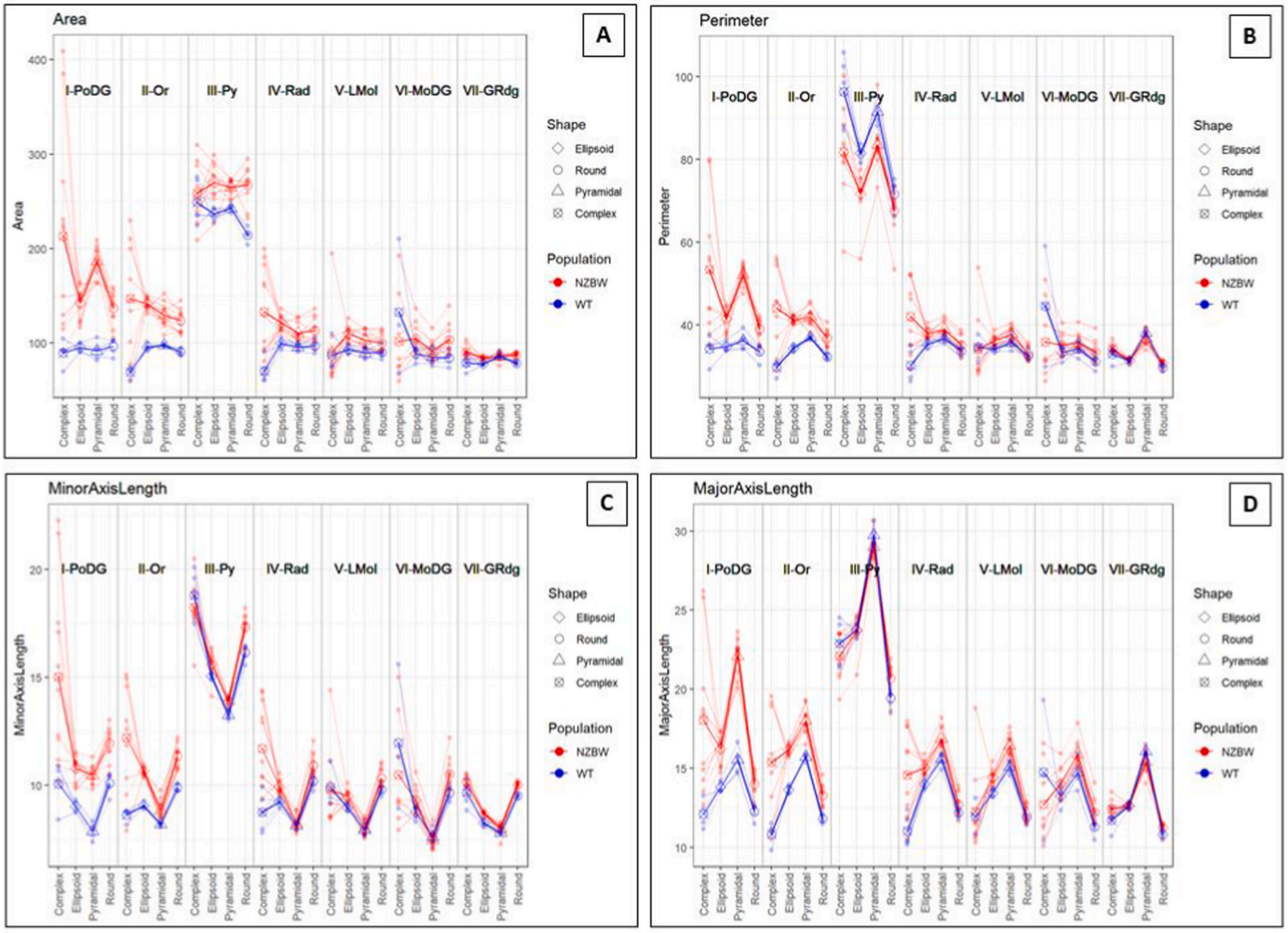

Fig. 2. Graphical representation of the Size morphometric descriptors. Results are presented by subject and by subregion, separately per cell shape types, in the two populations NZBW (red lines) and WT (blue lines). In A, plot of the area (in micons^2). In B, plot of the perimeter (micons). In C, plot of minor axis length. The parameter "minor axis length" corresponds to the length of the minor axis of the cell body expressed in µm. In D, plot of major axis length. The parameter major axis length corresponds to the length of the major axis of the cell body expressed in µm. The mean values for each morphometric descriptor are reported for the NZBW mice (red bold line) and for the WT mice (blue bold line). (For interpretation of the references to color in this figure legend, the reader is referred to the Web version of this article.)

2.7. Statistical analysis

The statistical analysis was performed comparing WT and NZBW populations for each domain within the 7 layers and the 4 shape types. As multiple cells recorded in each image are not independent, resampling-based the method proposed by Finos and Basso (2014) was used to account for repeated measures. The method is as follows: each image the mean of each feature is computed and used as pseudo-observation. The pseudo-observations are now independent, but not homoscedastic. They are randomly permuted among groups, while an adequate test statistics accounts for the heteroscedasticity. The p-value is the proportion of test statistics computed on randomly permuted pseudo-observations that exceeds the one computed on observed data.

This approach takes into account the joint distribution of the tests and allows for the multivariate inference via nonparametric Fisher combination of the univariate test. The tests are combined by morphometric descriptors, subregion and cell type. Significance level was set to alpha = 0.05. The analysis was performed with R software (R Core Team, 2021) and flip package (Finos and Basso, 2014). For descriptive purposes, a Principal Component Analysis was performed for each layer after standardization of the morphometric descriptors. A bi-plot of the first two principal components was drawn also reporting the explained variance of each component.

3. Results

3.1. Lamination of the hippocampal region and subregion

The DG, CA1, CA2 and CA3 regions were identified as well as the 7 subregions PoDG, Or, Py, Rad, LMol, MoDG and GrDG and their cytoarchitecture, in all mice (Fig. 1). Within each subregion, the 4 categories of cells type (pyramidal, round, ellipsoid and complex) were found in both NZBW and WT population. The general anatomy of the hippocampus followed its well-known description (Fig. 1).

3.2. Neurons in the NZBW hippocampus showed larger body size than WT neurons

The cells in the hippocampal neurons of NZBW mice were larger than neurons of WT mice in all subregions (Fig. 2). The Py subregion, where neurons had a larger perimeter in WT than NZBW mice, was an exception. Representation of the results, separately for each morphometric descriptor are shown in Fig. 2. Inferential analysis demonstrated a

strongly statistically significant difference ($p \leq 0.01$) in NZBW mice in the PoDG, Or, Py, Rad subregions, and a statistically significant difference ($p \leq 0.05$) in the GrDG and LMol subregions (Table 1). No difference in the size of neurons was found in the MoDg or the GrDG subregion. The analysis performed by categories and by subregion revealed which cell shape type contributed to the statistical significance (Table 1).

Details of the mean difference and standard error are reported separately for each morphometric descriptor in the section "Additional statistical results, (Supplementary Material). Moreover, detailed results of the p-values combined for domains subregions, cell shape and morphometric descriptor are reported in the in the section "Additional statistical results", (Supplementary Material).

3.3. WT mice showed a distinct clustering compared to NZBW for the domain size

The principal components analysis score plot was applied to visualize the sample distribution patterns (Fig. 3). The two-dimensional scatter plot was defined by the first and second principal components (PC1 and PC2, respectively). In all subregions except the MoDG, the NZBW mice were clearly separated from WT. In the PoDg, OR Py Rad and LMol subregions, the PC1 and 2 accounted for >80% of the total variance, indicating that WT subjects were well distinguished from NZBW, accounting for a large part of the statistically significant differences between them (Fig. 3).

3.4. Neurons in the hippocampus of NZBW mice showed more regular cell shape than WT neurons

The results for the Regularity morphometric descriptors revealed that NZBW neurons were more regular ($p \leq 0.01$) than WT neurons in all subregions (Fig. 4).

Inferential results obtained separately for each shape type revealed that round, ellipsoid and pyramidal cell contributed strongly ($p \leq 0.01$) to the statistical difference, while the complex shape type did not show differences (Table 2). Again, graphically, the Py neurons seemed to differ more between them and across cell shape.

3.5. Principal component analysis of NZBW populations and WT populations for the regularity domain

In all subregions, the PCA demonstrated a clear segregation of the WT and NZBW populations (Fig. 5). In Rad, PoDG but most prominently

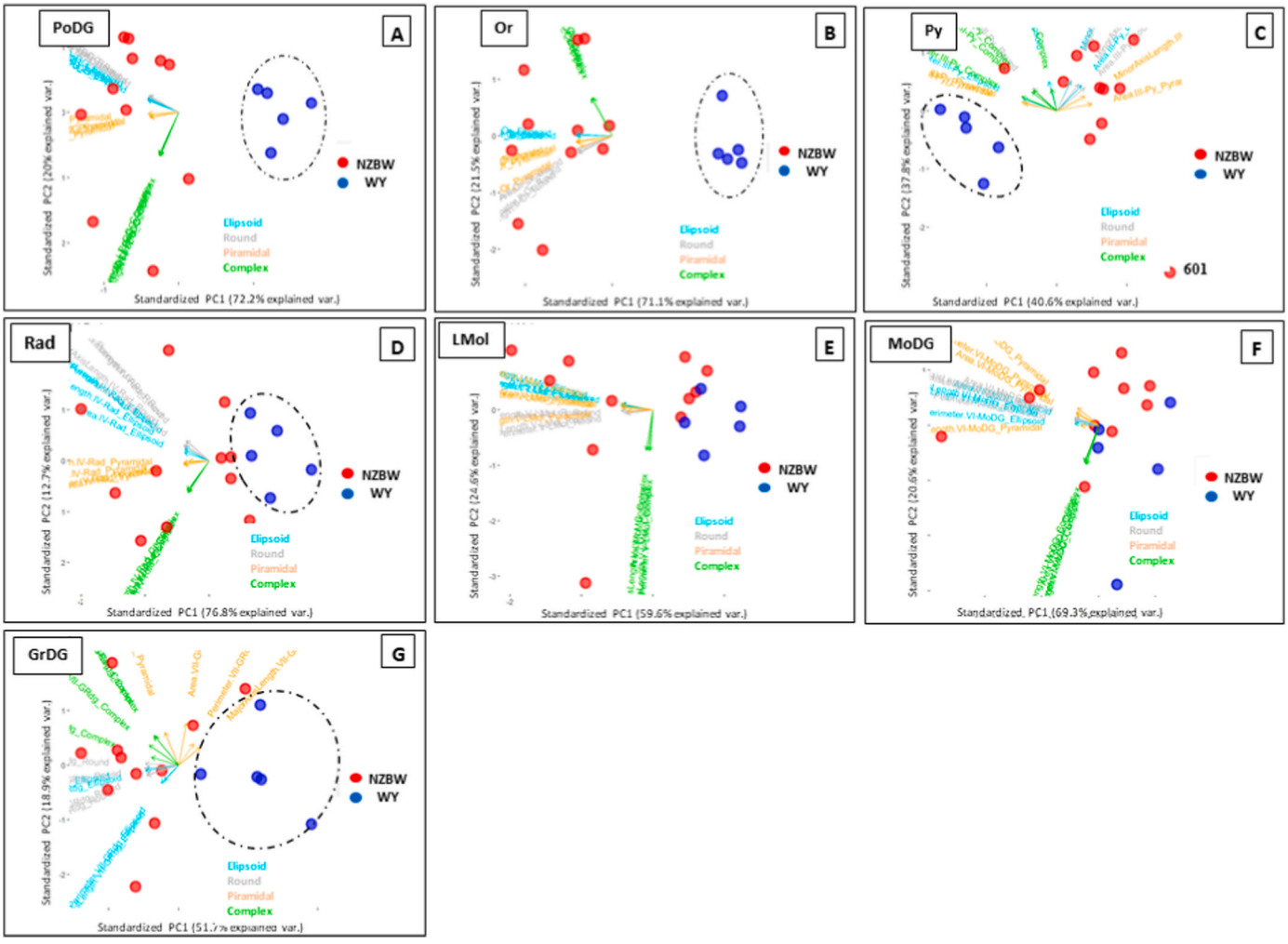

Fig. 3. Plot of the first (x-axis) against second (y-axis) PCA, for the Size domain, separated for each subregion, showing similarities (closer points) and differences (distant points) between each of the subjects bi-dimensionally separately for hippocampal subregion: in the plot A the PoDG; in B the Or, in C the Py, in D the Rad, in E the LMol, in F the MoDG, in G the GrDG. Each data point corresponds to one subject in function of the first two principal components of the morphometric descriptors. The single subjects resulted grouped by multiple inter-correlated variables and for the four types of cells shape considered (light blue, green, gray and yellow color). NZBW mice (red dots) and WT mice (blue dots). (For interpretation of the references to color in this figure legend, the reader is referred to the Web version of this article.)

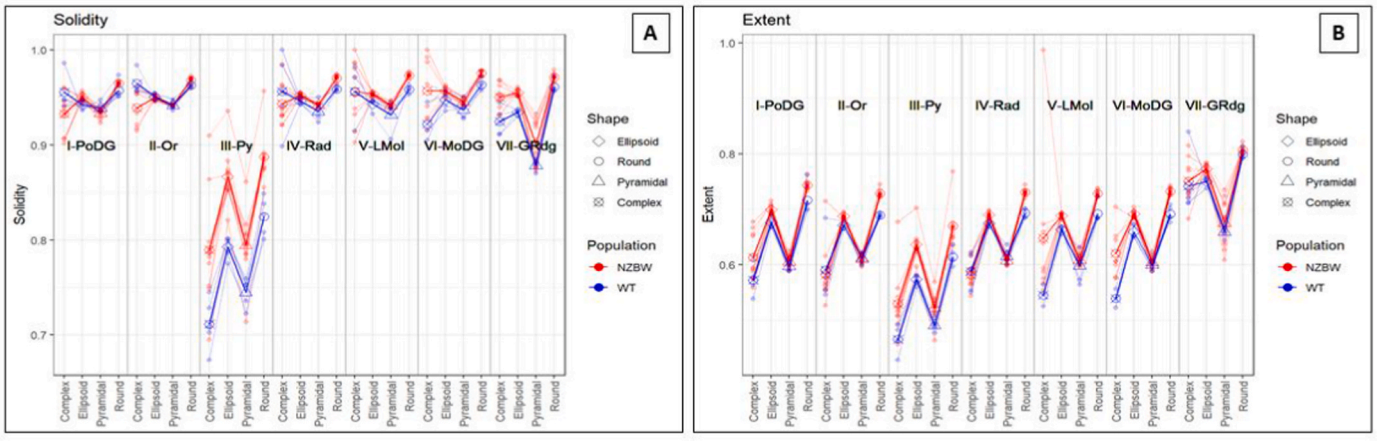

Fig. 4. Graphical representation of the Regularity morphometric descriptors solidity (plot A) and extent (plot B). Results are described by subject and by subregion, separately per cell shape types; NZBW (red lines) and WT (blue lines). The mean value for each morphometric descriptor is reported for the NZBW mice (red bold line) and for the WT mice (blue bold line). (For interpretation of the references to color in this figure legend, the reader is referred to the Web version of this article.)

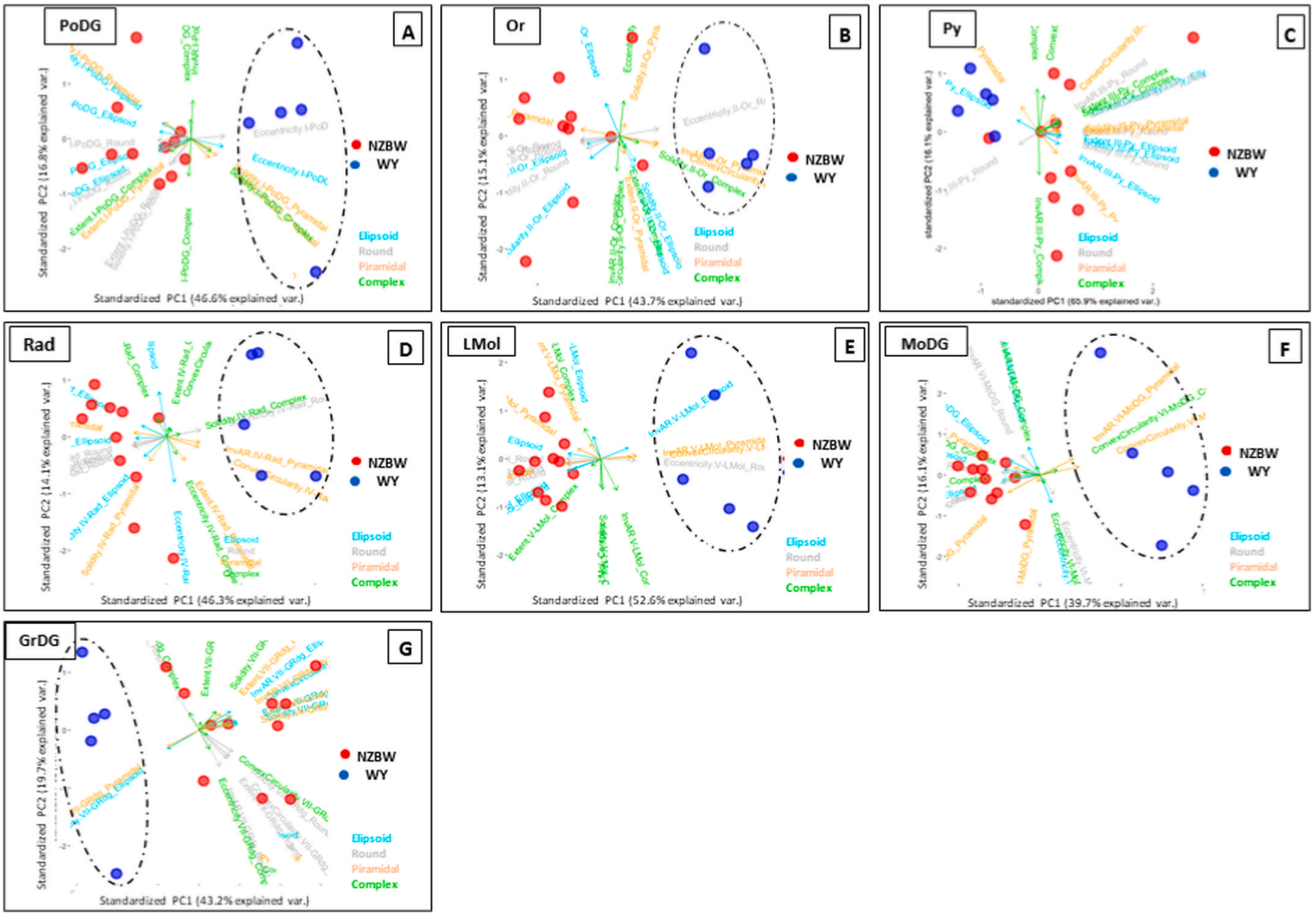

Fig. 5. Plot of the first (x-axis) against second (y-axis) PCA, for the Regularity domain, separated for each subregion, showing similarities (closer points) and differences (distant points) between each of the subjects bi-dimensionally: in the plot A the PoDG; in B the Or, in C the Py, in D the Rad, in E the LMol, in F the MoDG, in G the GrDG. Each data point corresponds to one subject in function of the first two principal components of the morphometric descriptors. The single subjects resulted grouped by multiple inter-correlated variables and for the four types of cells shape considered (light blue, green, gray and yellow color). NZBW mice (red dots) and WT mice (blue dots). (For interpretation of the references to color in this figure legend, the reader is referred to the Web version of this article.)

in Lmol and MoDG, the NZBW were closely clustered while WT were more widely distributed. In the Or and Py subregions, WT subjects formed a homogeneous group, while the subjects of the NZBW population exhibited a much wider distribution.

3.6. Neurons in the hippocampus of NZBW mice were denser than neurons in WT

NZBW neurons were denser than WT in most cases, except in Py and GrDG subregion (Fig. 6). The NZBW mice presented higher cell density in the Or, Rad, LMol and MoDG than the WT mice (Fig. 6). Multivariate analysis indicated a strong statistically significant difference ($p \leq 0.01$) in the Py, Rad LMol and MoDG, and statistically significant in Or ($p \leq 0.05$, Table 3).

Interestingly, the density in the Py subregion was lower in NZBW than in WT, and that was true for all the cell shape types (Fig. 6). The PoDG and GrDG subregions did not significant variation in cells density between the two mice populations (Table 3). In MoDg, Or and Lmol, the complex shapes were not significantly different from WT; neither were the pyramidal cells in MoDG.

3.7. Principal component analysis of NZBW populations and WT populations for the density domain

The PCA showed that, in Py and Lmol, NZBW mice formed a very homogeneous group while WT subjects revealed a more spread-out distribution (Fig. 7).

The subjects of the NZBW population in the Py subregion formed a well-defined group (Fig. 7). Control mice were homogeneous and close to each other in the Py, Lmol and MoDG. The two groups were clearly demarcated in the context of the Py, the Lmol and relatively so in the MoDG where the PC1 explained 97.5%, 74.6% and 78.2% of the variance, respectively. This was not the case in PoDG, Or, Rad and GrDG, (Fig. 7). In Py and Lmol specifically, the two populations seemed most segregated.

3.8. Summary of results

- **Size**: NZBW hippocampal neurons were larger in size than those of WT. No differences were found in the MoDg and GrDG subregion.
- **Regularity**: NZBW hippocampal neurons were significantly more regular than those of WT mice in all the subregions. However, the complex cell shape did not contribute to the statistical significance in any subregion.
- **Density**: In NZBW, neurons were usually denser than in WT. Interestingly, Py neurons were much denser in WT than in NZBW. The PoDG and GrDG did not show difference in cell density.

4. Discussion

This study is aimed at investigating alterations in the internal hippocampal cytoarchitecture of the NZBW mice lupus model. Our results revealed that neurons in the hippocampus of NZBW mice were denser, larger and showed a more a regular cell body than WT mice, apart in the Py subregion, where density of NZBW neurons was lower than in WT. Finally, PCA allow to distinguish healthy WT subjects from NZBW subjects.

4.1. How does NPSLE induce hippocampal damage? Two alternative hypotheses

The studies performed on possible hippocampal damages in both human SLE patients and in lupus mice models highlighted two alternative hypotheses: one suggests that NPSLE induces hippocampal damage and atrophy by either reducing the number of neurons (Ballok et al., 2004) or reducing the volume of the hippocampal structures (Appenzeller et al., 2006; Bódi et al., 2017; Liu et al., 2020). Conversely, the other hypothesis also proposes that NPSLE causes hippocampal damages, but increasing the local volumes, cells hypertrophy, and cells number (Zimmermann et al., 2017l). Other works have argued that, regarding the whole brain, volumetric variations do not scale well with alterations in cognitive abilities, and that the total number of neurons appears to be a much more accurate predictor of cognitive ability (Herculano-Houzel, 2011).

Recently, efforts have been focused on the involvement of microglia in NPSLE cognitive dysfunction, revealing an aberrant overexpression of these cells in lupus mice hippocampi (Qiao et al., 2021). Additionally, Grovola and colleagues assessed neuropathological and neuroinflammatory changes in subregions of the dentate gyrus of the pig (Grovola et al., 2020). They found mossy cell hypertrophy with a statistically significant increase in neuron density, specifically in the

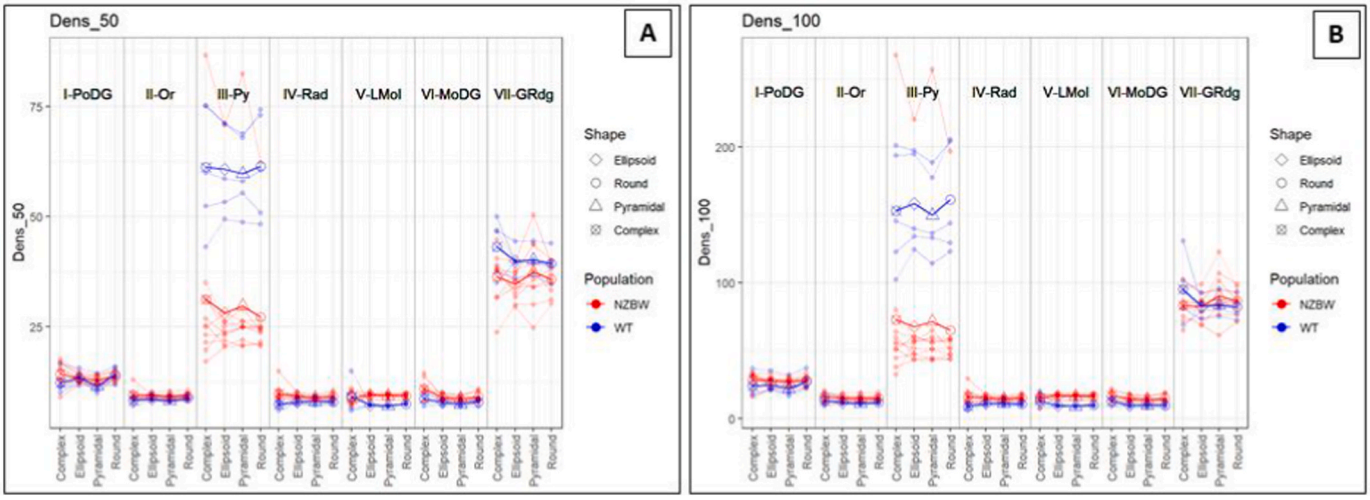

Fig. 6. Graphical representation of the morphometric descriptors Ngb_50 (plot A) and Ngb_100 (plot B), belonging to the Density domain. Results are described by subject and by subregion, separately per the cell shape types; NZBW (red lines) and WT (blue lines). The mean value for each morphometric descriptor is reported for the NZBW mice (red bold line) and for the WT mice (blue bold line). (For interpretation of the references to color in this figure legend, the reader is referred to the Web version of this article.)

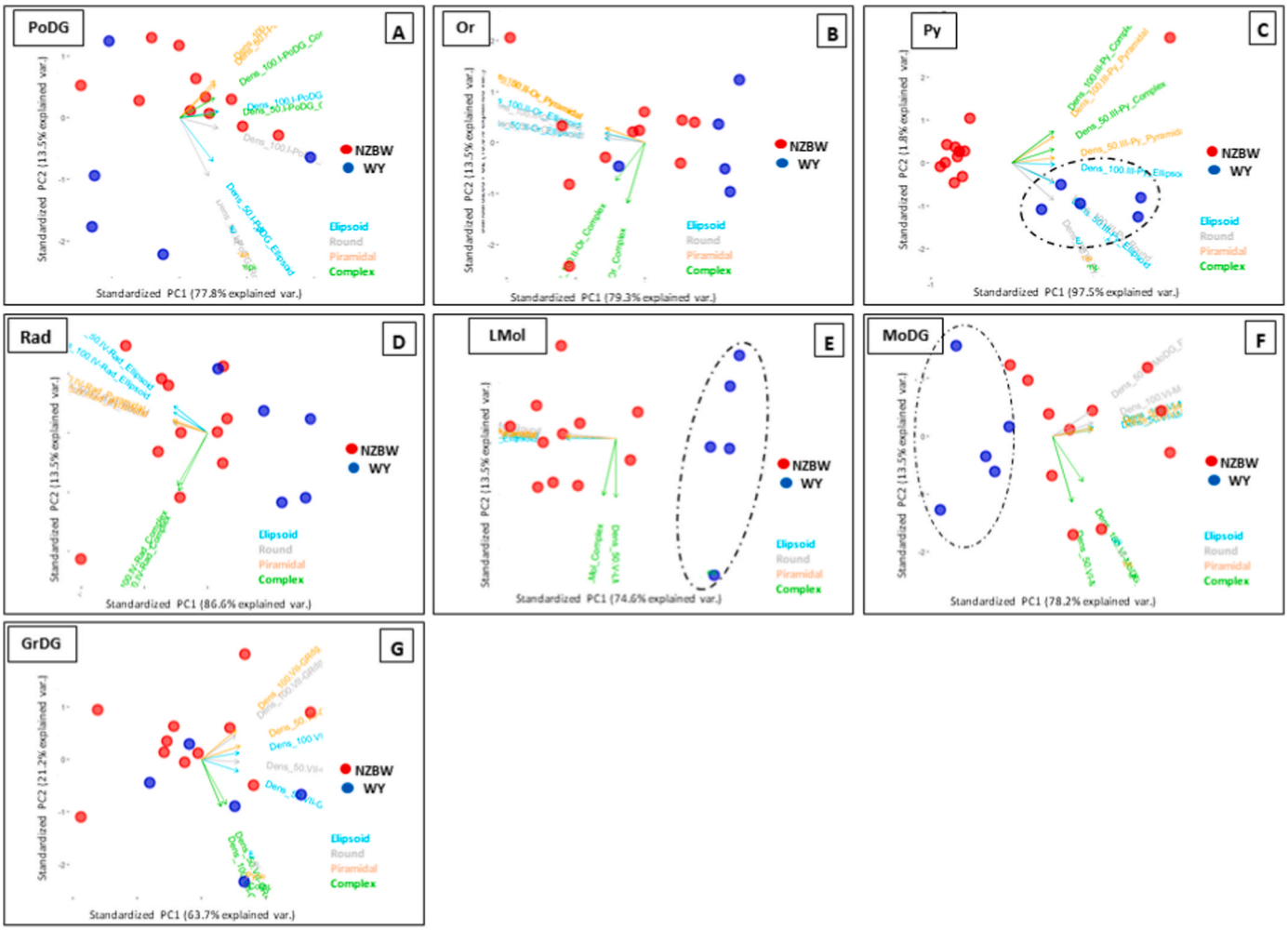

Fig. 7. Plot of the first PCA versus the second, for the Density domain, showing the be-dimensional visualization of similarities and differences between each of the subjects. Each point corresponds to one subject with a 2-D (the first two principal components) projection of the morphometric descriptors. The single subjects resulted grouped by multiple inter-correlated variables and for the four types of cells shape considered (light blue, green, gray and yellow color). NZBW mice (red dots) and WT mice (blue dots). (For interpretation of the references to color in this figure legend, the reader is referred to the Web version of this article.)

MoDG, at 7, 30 days and 1-year post brain injury, suggesting that microglial activation after brain injury may play a role in hippocampal circuit and/or synaptic remodeling (Grovola et al., 2020).

Despite contrasting results resulting in two hypotheses, most of these studies provide evidence on the presence of structural abnormalities in the brain linked to NPSLE manifestations. Whether neuron morphology might be affected and, eventually, which types or groups of neurons may be responsible for the differential effects on cognitive ability remains a subject of debate. The reason behind different and sometime contrasting results (Ota et al., 2022) could be related to the fact that no unifying pathophysiological processes has been found in the etiology of NPSLE.

Using advance quantitative imaging and statistical methods, over a large number of cells, we contributed to the discussion with hard evidence, showing as NZBW hippocampus possess cells hypertrophy (denser and larger neurons) than WT mice.

This finding support the hypothesis that NPSLE causes hippocampal cells hypertrophy. Conversely, the Py subregion in NZBW mice present lower density than in WT mice supporting the hypothesis that NPSLE induce hippocampal damage by reducing the number of neurons.

4.2. *Analysis combined by subregion and by cell shape allowed to highlight hidden differences*

We carried out the present analysis separately for the 7 hippocampal subregions, considering 4 types of neuronal shape. Using this focal approach, we were able to identify the hippocampal subregions in which the cytoarchitecture was altered and the type of neurons involved. An accurate account of the internal hippocampal cytoarchitecture is a key step towards the elucidation of the pathogenic mechanisms underlying NPSLE and virtually in all neurological disorders. In this sense the characterization of neuronal morphometry *via* descriptors at the cytoarchitecture meso-scale of an organ or a layer appears to be a powerful indicator of neural cells functions in health *vs.* pathology (Herculano-Houzel, 2011).

4.3. *The NZBW mice had larger body size and were denser than WT mice in PoDG, Or, Py, Rad, LMol*

The Or, Rad and LMol subregions are relatively cell-free areas containing subpopulations of interneurons. An interesting aspect in the LMol subregions is the presence of specific interneurons type, the so-called neuroglia-form cells that mediate powerful inhibition of CA1 pyramidal cells (Capogna 2011). These interneurons play an important role in the regulation of local circuits in the hippocampus proper, selectively regulating specific groups of neurons to enhance their function or protect vulnerable neurons from damage (Houser, 2007). Our results show that interneurons density and soma size tended to increase in the Or, Rad and LMol subregions of NZBW mice. Despite the lack of

data regarding interneuron morphology of patients with SLE or in lupus mice models, evidence of hypertrophy of interneurons in the hippocampus were described in several neuropathological conditions, including mice after epiloptogenetic hippocampal lesion (Sieu et al., 2017) and in the mouse model for the neurodegenerative disorder's neuronal ceroid lipofuscinoses (Cooper et al., 1999).

Pyramidal neurons are responsible to provide organized responses to spatial stimuli, non-spatial stimuli, and time in the Py subregions (Lisman et al., 2017). An increase in the soma size of the pyramidal neurons associated to cytoplasmic accumulations of phosphorylated neurofilament was demonstrated in neuropathological condition as hippocampal sclerosis in human (Thom et al., 1999). Hypertrophy of the hippocampus associated with an increase in perikarya size of pyramidal neurons was found also in transgenic synRas mice (Gärtner et al., 2004), suggesting an involvement of the Ras-signaling (Rat sarcoma virus) in morpho-regulatory and structural maintenance of hippocampal pyramidal neurons.

In prior works, variation in cell regularity have been considered to evaluate damages in brain areas due to ischemia or to highlight differences in cerebellum of bovine affected from Freemartin syndrome.

Leyh and colleagues, in the murine hippocampus and neocortex analyzed shape and regularity of cells (convex areas, circularities and other parameters) between control hemisphere and ischemic-affected hemisphere. They showed as microglia cells had larger convex hull area and soma circularities, within the control hemisphere compared to the ischemic-affected hemisphere (Leyh et al., 2021).

In a recently work Corain and colleagues set up a method to analyzed the cell shape, regularity and density in bovine cerebellar neurons, to quantify dimorphism in the cytoarchitecture among male, female and bovine affected from the freemartin syndrome, showing as the Freemartin granule neurons were the largest, most regular and dense (Corain et al., 2020).

4.4. No difference was found in neural density among NZBW and WT mice in the PoDG and GrDG subregion

Differences in neural density between NZBW and WT mice were not significant in the GrDG subregion. A possible explanation of the steady state of granule cells number in NZBW could be the result of the turnover process due to neurogenesis well described in the dentate gyrus of adult mammals (Amaral et al., 2007; Abbott and Nigussie, 2020). Although evidence indicate that neurogenesis in the dentate gyrus persists in the adult mammalian brain and appears to be under environmental control, (Abbott and Nigussie, 2020), studies have shown that the total number of granule cells does not vary in adult animals (Abbott and Nigussie, 2020), demonstrating that there is a steady state turnover of granule cells rather than a continuous accretion. These could explain way no difference was found in GrDG neural density between NZBW and WT mice.

The axons of the excitatory granule neurons in the GrDG reach direct to mossy cells in the PoDG (Scharfman, 2016). The loss of mossy cells, which are excitatory neurons making synaptic contact with granule cells, basket cells, and CA3 pyramidal neurons, has been demonstrated to contribute to DG dysfunction (Scharfman, 2016), resulting in the dysregulation of granule cell excitability, which in turn leads to abnormal behaviors such as anxiety and impaired pattern separation (Jinde et al., 2012).

4.5. WT subjects formed a defined cluster from the scattered NZBW subjects

The PCA analysis grouped the subjects, distinguishing WT subjects from NZBW subjects. Furthermore, it is worth noting that the variability among subjects within NZBW population was much larger than in WT mice.

The variability within NZBW subjects could be mainly due to multisystem involvement and confounding aspects (proteinuria levels) that occur in lupus disease. These multisystem aspects could also be the reason why experimental studies have not yet been able to explain the main causes and mechanisms involved in the pathogenesis of NPSLE (Bruyn, 1995).

The PCA method is useful when data sets from different modalities are combined or if the analysis is complex that there is a need for dimension reduction. Despite is very difficult to clarify how neuroanatomical changes are relating to clinical symptoms of **neurodegenerative diseases**, the PCA showed the possibility to differentiate healthy patients from schizophrenic patients (Caprihan et al., 2008; Rotarska--Jagiela et al., 2008). The application of PCA was proposed also to improve the performance of Alzheimer's disease detection (Suresha and Parthasarathy, 2021).

Recently, in the field of SLE, the PCA performed well in lupus nephritis patients, identifying important risk factors and thus enabling clinicians to identify subjects at-risk and either implement preventative strategies or manage current treatments (Huang et al., 2020). The PCA was also used to determine which groups of cytokines have the greatest influence across disease activity states helping to describe the influence of complex cytokine interactions in SLE (Raymond et al., 2019). The PCA was also applied as a tool to identify lesioned skin patterns in cutaneous lupus erythematosus, helping to characterize where on the body lesions of cutaneous lupus erythematosus tend to occur in patients (Prasad et al., 2020).

The methodology we propose based on in-depth analysis of the morphology of neural cells, provides a collection of valuable data on the morphology of multiple cells, acquired and analyzed individually. In the context of the investigation of pathological changes in structures of the brain areas, due to SLE disease, the application of PCA as technique for reducing the dimensionality of such datasets, allows the increasing interpretability but at the same time minimizing information loss. The collection of large datasets are increasingly common in pathological investigation and the method we proposed could be a powerful tool to distinguish healthy from pathological neurons in postmortem sample analysis.

5. Conclusion

The methodology we set-up consists of multivariate and multi-aspect testing for cytoarchitecture-ranking, based on neuronal cell shape analysis, among populations defined by factors, such as sex, age or pathology. This tool could be a powerful instrument to carry out morphometric analysis providing a robust basis for objective tissue screening, especially in the field of neurodegenerative pathologies.

The analysis carried out separately for each hippocampal subregion provided a baseline to highlight hidden effects on the neuronal cytoarchitecture with respect to analyses conducted without this subdivision.

The application of PCA methodology represents a possible approach to understanding the effects of lupus disease in the brain, optimizing the interpretation of complex data in diagnostics of neurolupus consequences.

Despite the statistically significant morphologic alterations that we found in the NZBW lupus mice hippocampal cytoarchitecture, it remains to be determined whether these structural modifications are associated with the progress of the autoimmune disease and whether these modifications are functionally important.

We are aware that the pathogenetic aspects of lupus in NZBW mice are not entirely representative of the of human pathology. However, this murine model can significantly contribute towards the understanding of lupus.

Ethics approval and consent to participate

All experimental procedures were previously approved by the

"Padova University Animal Ethic Committee and Italian Ministry of Health with the authorization number 720/2017-PR under the Italian Law Dlgs 26/2014".

Authors' contributions

Antonella Peruffo: Conceptualization, Supervision, Writing, Original draft, Writing - review & editing. Jean-Marie Graïc: Conceptualization, Methodology, Writing - review & editing. Tommaso Gerussi: Methodology, Writing - review & editing. Bruno Cozzi: Conceptualization, Writing - review & editing. Andrea Doria: Conceptualization, Writing - review & editing. Mariella Gatto: Writing - review & editing. Livio Finos: Methodology, Writing - review & editing. Livio Corain: Methodology, Writing - review & editing. Roberto Luisetto: Conceptualization, Writing - review & editing. Enrico Grisan: Methodology, Supervision, Writing - review & editing.

Funding

This study was supported by a University of Padova Grant (BIRD # 179299/17) to Antonella Peruffo.

Consent to publication

The authors declare that they consent to publication.

Declaration of competing interest

The authors declare that they have no known competing financial interests or personal relationships that could have appeared to influence the work reported in this paper.

Data availability

Data will be made available on request.

Acknowledgements

Not applicable.

Abbreviation

NZB/W F1 (NZBW)
Systemic Lupus Erythematosus (SLE)
Central nervous system (CNS)
Neuropsychiatric SLE (NPSLE)
Dentate gyrus (DG)
Molecular layer (MoDG)
Granule cell layer (GrDG)
Polymorph dentate gyrus (PoDG)
Pyramidal layer (Py)
Stratum oriens (Or)
Stratum radiatum (Rad)
Stratum lacunosum-moleculare (LMol)

Appendix A. Supplementary data

Supplementary data to this article can be found online at https://doi.org/10.1016/j.bbih.2023.100662.

References

Abbott, L.C., Nigussie, F., 2020. Adult neurogenesis in the mammalian dentate gyrus. Anat. Histol. Embryol. 49 (1), 3–16. https://doi.org/10.1111/ahe.12496.

Amaral, D.G., Scharfman, H.E., Lavenex, P., 2007. The dentate gyrus: fundamental neuroanatomical organization (dentate gyrus for dummies). Prog. Brain Res. 163, 3–22. https://doi.org/10.1016/S0079-6123(07)63001-5.

Appenzeller, S., Carnevalle, Li, L.M., Costallat, L.T.L., Cendes, F., 2006. Hippocampal atrophy in systemic lupus erythematosus. Ann. Rheum. Dis. 65, 1585–1589. https://doi.org/10.1136/ard.2005.049486.

Ballok, D.A., Woulfe, J., Sur, M., Cyr, M., Sakic, B., 2004. Hippocampal damage in mouse and human forms of systemic autoimmune disease. Hippocampus 14 (5), 649–661.

Bódi, N., Polgár, A., Kiss, E., Mester, Á., Poór, G., Kéri, S., 2017. Reduced volumes of the CA1 and CA4-dentate gyrus hippocampal subfields in systemic lupus erythematosus. Lupus 26 (13), 1378–1382. https://doi.org/10.1177/0961203317701845.

Briani, C., Lucchetta, M., Ghirardello, A., Toffanin, E., Zampieri, S., Ruggero, S., Scarlato, M., Quattrini, A., Bassi, N., Ermani, M., Battistin, L., Doria, A., 2009. Neurolupus is associated with anti-ribosomal P protein antibodies: an inception cohort study. J. Autoimmun. 32 (2), 79–84. https://doi.org/10.1016/j.jaut.2008.12.002.

Bruyn, G.A., 1995. Controversies in lupus: nervous system involvement. Ann. Rheum. Dis. 54, 159–167.

Capogna, M., 2011. Neurogliaform cells and other interneurons of stratum lacunosum-moleculare gate entorhinal–hippocampal dialogue. J. Physiol. 589 (Pt 8), 1875–1883. https://doi.org/10.1113/jphysiol.2010.201004.

Caprihan, A., Pearlson, G.D., Calhoun, V.D., 2008. Application of principal component analysis to distinguish patients with schizophrenia from healthy controls based on fractional anisotropy measurements. Neuroimage 42 (2), 675–682. https://doi.org/10.1016/j.neuroimage.2008.04.255.

Cooper, J.D., Messer, A., Feng, A.K., Chua-Couzens, J., Mobley, W.C., 1999. Apparent loss and hypertrophy of interneurons in a mouse model of neuronal ceroid lipofuscinosis: evidence for partial response to insulin-like growth factor-1 treatment. J. Neurosci. 19 (7), 2556–2567. https://doi.org/10.1523/JNEUROSCI.19-07-02556.1999.

Corain, L., Grisan, E., Graïc, J.M., Carvajal-Schiaffino, R., Cozzi, B., Peruffo, A., 2020. Multi-aspect testing and ranking inference to quantify dimorphism in the cytoarchitecture of cerebellum of male, female and intersex individuals: a model applied to bovine brains. Brain Struct. Funct. 225 (9), 2669–2688. https://doi.org/10.1007/s00429-020-02147-x.

Finos, L., Basso, D., 2014. Permutation tests for between-unit fixed effects in multivariate generalized linear mixed models. Stat. Comput. 24 (6), 941–952.

Gärtner, U., Alpár, A., Reimann, F., Seeger, G., Heumann, R., Arendt, T., 2004. Constitutive Ras activity induces hippocampal hypertrophy and remodeling of pyramidal neurons in synRas mice. J. Neurosci. Res. 1 (5), 630–641. https://doi.org/10.1002/jnr.20194, 77.

Gatto, M., Ghirardello, A., Luisetto, R., Bassi, N., Fedrigo, M., Valente, M., Valentino, S., Del Prete, D., Punzi, L., Doria, A., 2016. Immunization with pentraxin 3 (PTX3) leads to anti-PTX3 antibody production and delayed lupus-like nephritis in NZB/NZW F1 mice. J. Autoimmun. 74, 208–216. https://doi.org/10.1016/j.jaut.2016.07.002.

Gatto, M., Radu, C.M., Luisetto, R., Ghirardello, A., Bonsembiante, F., Trez, D., Valentino, S., Bottazzi, B., Simioni, P., Cavicchioli, L., Doria, A., 2020. Immunization with Pentraxin3 prevents transition from subclinical to clinical lupus nephritis in lupus-prone mice: insights from renal ultrastructural findings. J. Autoimmun. 111, 102443 https://doi.org/10.1016/j.jaut.2020.102443.

Ghirardello, A., Doria, A., Zampieri, S., Tarricone, E., Tozzoli, R., Villalta, D., Bizzaro, N., Piccoli, A., Gambari, P.F., 2004. Antinucleosome antibodies in SLE: a two-year follow-up study of 101 patients. J. Autoimmun. 22 (3), 235–240. https://doi.org/10.1016/j.jaut.2003.12.005.

Grisan, E., Graic, J.-M., Corain, L., Peruffo, A., 2018. Resolving single cells in heavily clustered Nissl-stained images for the analysis of brain cytoarchitecture. In: 2018 IEEE 15th International Symposium on Biomedical Imaging (ISBI 2018). IEEE, pp. 427–430. https://doi.org/10.1109/ISBI.2018.8363608.

Grovola, M.R., Paleologos, N., Wofford, K.L., Harris, J.P., Browne, K.D., Johnson, V., Duda, J.E., Wolf, J.A., Cullen, D.K., 2020. Mossy cell hypertrophy and synaptic changes in the hilus following mild diffuse traumatic brain injury in pigs. J. Neuroinflammation 17 (1), 44. https://doi.org/10.1186/s12974-020-1720-0.

Hainmueller, T., Bartos, M., 2020. Dentate gyrus circuits for encoding, retrieval and discrimination of episodic memories. Nat. Rev. Neurosci. 21 (3), 153–168. https://doi.org/10.1038/s41583-019-0260-z.

Suresha, Halebeedu Subbaraya, Parthasarathy, Srirangapatna Sampathkumaran, 2021. Probabilistic principal component analysis and long ShortTerm memory classifier for automatic detection of Alzheimer's disease using MRI brain images. J. Inst. Eng. India Ser. B 102 (4), 807–818. https://doi.org/10.1007/s40031-021-00571-z.

Herculano-Houzel, S., 2011. Brains matter, bodies maybe not: the case for examining neuron numbers irrespective of body size. Ann. N. Y. Acad. Sci. 1225, 191–199.

Huang, T., Li, J., Zhang, W., 2020. Application of principal component analysis and logistic regression model in lupus nephritis patients with clinical hypothyroidism. BMC Med. Res. Methodol. 20 (1), 99. https://doi.org/10.1186/s12874-020-00989-x.

Jarsky, T., Roxin, A., Kath, W.L., Spruston, N., 2005. Conditional dendritic spike propagation following distal synaptic activation of hippocampal CA1 pyramidal neurons. Nat. Neurosci. 8 (12), 1667–1676.

Jinde, S., Zsiros, V., Jiang, Z., Nakao, K., Pickel, J., Kohno, K., et al., 2012. Hilar mossy cell degeneration causes transient dentate granule cell hyperexcitability and impaired pattern separation. Neuron 76, 1189–1200.

Kowal, C., DeGiorgio, L.A., Nakaoka, T., Hetherington, H., Huerta, P.T., Diamond, B., Volpe, B.T., 2004. Cognition and immunity; antibody impairs memory. Immunity 21 (2), 179–188. https://doi.org/10.1016/j.immuni.2004.07.011.

Leung, J.W., Lau, B.W., Chan, V.S., Lau, C.S., So, K.F., 2016. Abnormal increase of neuronal precursor cells and exacerbated neuroinflammation in the corpus callosum in murine model of systemic lupus erythematosus. Restor. Neurol. Neurosci. 34 (3), 443–453. https://doi.org/10.3233/RNN-160638.

Leyh, J., Paeschke, S., Mages, B., Michalski, D., Nowicki, N., Bechmann, I., Winter, K., 2021. Classification of microglial morphological phenotypes using machine learning. Front. Cell. Neurosci. 15, 701673 https://doi.org/10.3389/fncel.2021.701673.

Lisman, J., Buzsáki, G., Eichenbaum, H., Nadel, L., Ranganath, C., Redish, A.D., 2017. Viewpoints: how the hippocampus contributes to memory, navigation and cognition. Nat. Neurosci. 20 (11), 1434–1447. https://doi.org/10.1038/nn.4661.

Liu, S., Cheng, Y., Zhao, Y., Lai, A., Lv, Z., Xie, Z., Upreti, B., Wang, X., Xu, X., Luo, C., Yu, H., Shan, B., Xu, L., Xu, J., 2020. Hippocampal atrophy in systemic lupus erythematosus patients without major neuropsychiatric manifestations. J. Immunol. Res. 2020, 2943848 https://doi.org/10.1155/2020/2943848.

Merino-Serra, P., Tapia-Gonzalez, S., DeFelipe, J., 2020. Calbindin immunostaining in the CA1 hippocampal pyramidal cell layer of the human and mouse: a comparative study. J. Chem. Neuroanat. 104, 101745 https://doi.org/10.1016/j.jchemneu.2020.101745.

Ota, Y., Srinivasan, A., Capizzano, A.A., Bapuraj, J.R., Kim, J., Kurokawa, R., Baba, A., Moritani, T., 2022. Central nervous system systemic lupus erythematosus: pathophysiologic, clinical, and imaging features. Radiographics 42 (1), 212–232. https://doi.org/10.1148/rg.210045.

Paxinos, G., Franklin, K., 2012. Paxinos and Franklin's the Mouse Brain in Stereotaxic Coordinates, third ed.

Pikman, R., Kivity, S., Levy, Y., Arango, M.T., Chapman, J., Yonath, H., Shoenfeld, Y., Gofrit, S.G., 2017. Neuropsychiatric SLE: from animal model to human. Lupus 26, 470–477.

Poletti, E., Zappelli, F., Ruggeri, A., Grisan, E., 2012. A review of thresholding strategies applied to human chromosome segmentation. Comput. Methods Progr. Biomed. 108 (2), 679–688. https://doi.org/10.1016/j.cmpb.2011.12.003.

Prasad, S., Raman, J., Ogunsanya, M.E., Chong, B.F., 2020. Principal components analysis as a tool to identify lesional skin patterns in cutaneous lupus erythematosus. J. Am. Acad. Dermatol. 83 (3), 922–924. https://doi.org/10.1016/j.jaad.2020.01.010.

Qiao, X., Wang, H., Lu, L., Chen, J., Cheng, Q., Guo, M., Hou, Y., Dou, H., 2021. Hippocampal microglia CD40 mediates NPSLE cognitive dysfunction in mice. J. Neuroimmunol. 357, 577620 https://doi.org/10.1016/j.jneuroim.2021.577620.

Raymond, W.D., Eilertsen, G.Ø., Nossent, J., 2019. Principal component analysis reveals disconnect between regulatory cytokines and disease activity in systemic lupus erythematosus. Cytokine. 114, 67–73. https://doi.org/10.1016/j.cyto.2018.10.013.

Rotarska-Jagiela, A., Schonmeyer, R., Oertel, V., Haenschel, C., Vogeley, K., Linden, D.E., 2008. The corpus callosum in schizophrenia-volume and connectivity changes affect specific regions. Neuroimage 39, 1522–1532.

Scharfman, H.E., 2016. The enigmatic mossy cell of the dentate gyrus. Nat. Rev. Neurosci. 17, 562–575.

Schwartz, N., Stock, A.D., Putterman, C., 2019. Neuropsychiatric lupus: new mechanistic insights and future treatment directions. Nat. Rev. Rheumatol. 15 (3), 137–152. https://doi.org/10.1038/s41584-018-0156-8.

Sieu, L.A., Eugène, E., Bonnot, A., Cohen, I., 2017. Disrupted Co-activation of interneurons and hippocampal network after focal Kainate lesion. Front. Neural Circ. 11, 87. https://doi.org/10.3389/fncir.2017.00087.

Thom, M., D'Arrigo, C., Scaravilli, F., 1999. Hippocampal sclerosis with hypertrophy of end folium pyramidal cells. Acta Neuropathol. 98 (1), 107–110. https://doi.org/10.1007/s004010051057.

Zaletel, I., Filipović, D., Puškaš, N., 2016. Chronic stress, hippocampus and parvalbumin-positive interneurons: what do we know so far? Rev. Neurosci. 27, 397–409.

Zimmermann, N., Goulart Corrêa, D., Tukamoto, G., Netto, T., Batista Pereira, D., Paz Fonseca, R., Gasparetto, E.L., 2017l. Brain morphology and cortical thickness variations insystemic lupus erythematosus patients: differences among neurological, psychiatric, and non-neuropsychiatric manifestations. J. Magn. Reson. Imag. 46 (1), 150–158. https://doi.org/10.1002/jmri.25538.